6.7 3D VELOCITY STRUCTURE AND FLUID FLOWS INFERRED FROM THE MICROSEISMIC EVENTS IN THE GEOTHERMAL FIELD, TURKEY

B. Turhan[1*], T. Bilgiç[2], Ü.S. Selek[2], K. Balcı[3], A. Yıldırım[3], B. Kaypak[4]

[1]TPAO,Nizami Gencevi Cad.,Çankaya,Ankara,Turkey
[2]Mikrosismik Mühendislik Danışmanlık Ltd.Sti.,Hacettepe Teknokent,Ankara,Turkey
[3] MASPO Energy San.and Tic.A.Ş.,Manisa,Turkey
[4] Jeofizik Mühendisliği Bölümü,Ankara Üniversitesi,Ankara,Turkey
**Corresponding author e-mail: buturhan@tpao.gov.tr*

ABSTRACT

Geothermal energy, being a renewable energy source, holds significant potential, particularly in our country. Once exploration methods are employed to identify suitable locations for production wells and the optimal placement of geothermal power plants, there is often a lack of further studies focused on reservoir monitoring or reservoir management within the field. However, it is crucial to implement microseismic monitoring as a customary practice to ensure the sustainability of geothermal reservoirs. This method has been extensively applied worldwide in various geothermal projects. Nonetheless, the first comprehensive application of this method in an industrial context in our country was carried out at the Manisa Geothermal site, supported by TÜBİTAK (1501 TÜBİTAK-TEYDEP Project no: 3200756). Initially, we selected seven borehole sensors strategically positioned around production and injection wells in the geothermal field based on noise analysis results. Continuous data records were analyzed to detect and locate microseismic events, calculate their magnitudes, and determine focal mechanism solutions for assessing stress changes. These events occurred underground during the operations of re-injection, production wells, and overall geothermal activities. Finally, 3D seismic tomography studies were conducted to determine the velocity structure of the field, the mapping of the current reservoir conditions, and the movement of water within the subsurface.

KEY WORDS: Geothermal Energy, Microseismic Monitoring, Reservoir Monitoring, Induced Seismicity.

INTRODUCTION

Renewable energy sources have garnered global significance due to the depletion of fossil fuels and the escalating demand for energy. Our country holds the highest potential with regards to geothermal resources. Geothermal energy is a renewable and environmentally friendly form of energy derived from natural heat sources situated deep within the Earth's crust. The production of geothermal energy involves the extraction of subterranean water or steam, which is subjected to high temperature and pressure, for the purpose of energy generation. During these operations, microseismic events occur, which are characterized by low energy, high frequency, small amplitude, and rapid attenuation.

The microseismic method entails the precise measurement of seismic wave characteristics, including velocity, frequency, and shape. The standardized implementation of this method is significant for the effective monitoring and management of geothermal reservoirs, ensuring safety and operational efficiency in geothermal field operations. Numerous academic and industrial studies have been conducted worldwide in this field. For instance, it has been used to estimate the spatiotemporal behavior of reservoirs, as demonstrated by studies such as Fehler et al. (1987) and Baria et al. (1999). In a seismic cluster in Basel, Switzerland, Asanuma et al. (2008) successfully determined the locations of microseismic events. The concept of diffusion in fluid-saturated rocks, as proposed by Shapiro et al. (1997), established a relationship between microseismic events and the advancement of the water front (Shapiro et al. 2002). Several studies have endeavored to elucidate pore-pressure migration by incorporating selective water flow in permeable fractures and faults, commonly referred to as the water flow model, as demonstrated by works such as Evans et al. (2005), McClure and Horne (2011), and Mukuhira et al. (2016).

Unfortunately, there is a lack of studies regarding the application of the microseismic method and reservoir monitoring through microseismic events in our country. This study represents the first comprehensive application of this method in our country, supported by TÜBİTAK. To record continuous data, seven borehole sensors were installed in the geothermal production area. The positioning of these stations was determined based on a noise analysis study, allowing for the elimination of background noise sources such as wind, ocean waves, tides, traffic, industrial activities, and artificial explosions (Tunc et al., 2023). Microseismic events were selected from a two-year dataset collected between July 2021 and July 2023. The locations of these events, along with their magnitude calculations and focal mechanism solutions, are presented to illustrate the current state of the reservoir and water flow path (Turhan et al., 2023). In addition, this study presents tomography results obtained through the analysis of the located microseismic events. These results enabled us to determine the velocity structure of the geothermal field and the current status of the reservoir.

GEOLOGICAL SETTING OF THE STUDY AREA

The study area is situated within the boundaries of the Alaşehir district in Manisa province, Turkey. The region is characterized by a combination of pre-Neogene basement rocks and Neogene and Quaternary sedimentary units. Information regarding the geology and stratigraphy of the study area has been compiled from various sources, including Karamanderesi (1994), Karahan (2007), Yolal and Karahan (2010), and Batum et al. (2012). The presence of ancient faults and graben tectonics, which originated during the closure of the Menderes Massif and the Izmir-Ankara Zone, represents significant geological structures within the region. Based on the overall geological framework, two distinct stratigraphic sequences have been identified in the study area. The lowermost units consist of basement rocks belonging to the Menderes metamorphic complex, which have undergone high-pressure and high-temperature metamorphism. Above the basement units are Tertiary sedimentary rocks. The youngest geological formations in the study area are travertines, which form at the outlets of hot and cold water sources, as well as old and recent alluvial deposits.

The study area represents a reservoir-like region situated within a geological formation known as the Gediz Graben. The Gediz Graben is a rift basin formed by continental rifting processes (Koçyiğit, 2000). During the Miocene period, the graben initially developed as a half-graben, with only the southern margin exhibiting active faulting. Subsequently, in the Plio-Quaternary period, the graben acquired its current asymmetric configuration with the activation of the fault system along the northern margin. The sediments deposited in front of the normal faults constitute the oldest sedimentary fill within the Gediz Graben (Yılmaz et al., 2000). In the study area, the Quaternary sediments can be classified as alluvial fan sediments, fluvial sediments, lacustrine sediments with intercalated fan deltas, and delta sediments. The tectonic structure of the Gediz Graben has significantly contributed to the geothermal potential observed in the region.

RESERVOIR MONITORING and MICROSEISMIC TOMOGRAPHY

In the initial phase of this study, we conducted the localization of microseismic events and determined their depth values by utilizing velocity information obtained from seismic reflection data collected in the field area. The arrival of P- and S-waves was manually identified, and precise hypocenter locations were determined using the Geiger algorithm (Geiger, 1910) and the HYPO2000 program (Klein, 2002). Upon analyzing the spatial distribution of event locations, it becomes evident that there is a higher concentration of events toward the north in the southern portion of the field. This suggests a greater occurrence of fractures during the movement of water in the southern section. This result implies that the lithological formations in the southern part of the field are more prone to fracturing, allowing the reservoir water to circulate at greater depths with less pressure. Another significant finding is that the depth range of the events falls within approximately 1-5 km, which corresponds to the depths associated with geothermal activity. To determine the size of fractures, duration magnitude calculation was employed. Examining the magnitude distribution of microseismic events, it can be observed that induced events with smaller magnitudes tend to occur in proximity to the production and injection wells, whereas naturally occurring tectonic events located at greater depths exhibit larger magnitudes. Figure 1 illustrates the microseismic events located, their magnitudes, and depth values over a two-year period.

Furthermore, focal mechanism solutions were computed for 115 events using the moment tensor inversion algorithm. The solutions indicate predominantly strike-slip faulting. The orientation of the fractures aligns with the geological structure of the field, trending in a northwest-southeast direction. This information allowed us to determine changes in stress distribution and the path of fluid flow within the reservoir. Moreover, we were able to track the distribution of microseismic events in relation to the activities of production and injection wells, thus gaining insights into the pressure and flow variations. It was observed that induced events often coincided with changes in well activity.

Subsequently, seismic travel wave tomography was conducted using microseismic events located over a two-year period. Three-dimensional seismic tomography involves recording the elastic waves emitted by seismic sources in a region using seismographs. The travel times of these seismic wave phases (P- and S-waves) were then subjected to a series of inverse solution processes to visualize the 3D seismic velocity structure of the subsurface. For this study, 1368 events were selected from the 1635 microseismic events detected between July 2021 and the June 2023. The selection process involved applying limited value criteria such as a gap value equal to or smaller than 300° and RMS values below 0.2. Consequently, 5555 P-wave travel time data and 5519 S-wave travel time data were used in the tomography analysis. This allowed us to estimate the P-wave velocity (VP), S-wave velocity (VS), and their ratio (VP/VS) based on a seismic wave tomography method.

Tomographic imaging of the field involved modeling based on the distribution of microseismic events and stations, the number of P- and S-phase readings within the dataset, and the depth variations of the events. The inversion grids employed for forward modeling had dimensions of 500×500×1000 m. The inverse solution process consisted of two steps. Initially, a 3D VP structure of the region was obtained using only P-wave travel times. The VP/VS structure was then obtained by referencing this VP structure and incorporating the S-wave travel times.

The 3D velocity structure composed of VP (P-wave velocity) and VP/VS (ratio of P-wave velocity to S-wave velocity) for the region was determined up to a depth of approximately 6 km. However, it should be noted that areas without seismic ray paths were unable to be imaged. The velocity values obtained along the existing ray paths can be considered to have lower error values and yield more realistic outcomes. Figure 2 illustrates the calculated ray paths employed in the tomography analysis. VP sections corresponding to specific depth intervals are displayed in Figure 3. Borehole station points are represented by triangles, well locations by rectangles, and events by points. In addition, the VP/VS sections for the selected depth intervals are presented in Figure 4. VP/VS values play a crucial role in interpreting reservoir conditions and fluid pathways, as they serve as important indicators of the fluid content within the reservoir. Higher VP/VS values are often associated with geothermal reservoirs dominated by hot water (Muksin et al., 2013). Conversely, the occurrence of a low VP/VS structure can be attributed to the depletion of pore liquid water and its replacement with steam, particularly in areas with low VP and high VS (Gunasekera et al., 2003). Another possible explanation for the low VP/VS structure is the presence of granite.

The prospective region extending westward from the AKU station, which is characterized by a high VP/VS velocity ratio, is of particular interest. This region coincides with areas where cracks and fractures are likely to occur due to water circulation, as evidenced by an increased number of microseismic events. Changes in the VP and VP/VS values along a selected longitude section are shown in Figure 5. Finally, to facilitate the 3D interpretation of the tomographic results, numerical data were visually represented volumetrically using an isosurface representation, as depicted in Figure 6. In the figure, anomalies that signify the presence of a reservoir and indicate the presence of fluid are believed to correspond to areas where the VP/VS ratio is elevated (light green and red volumetric areas). These anomalies are predominantly located in the southern part of the area, within depth intervals of approximately 2–6 km.

CONCLUSION

The data used in this study were collected over a 24-month period through the deployment of seven borehole sensors within the study area. A total of 1635 microseismic events were selected from continuous passive seismic records. Notably, these events were found to be predominantly concentrated in the southern part of the field rather than in the northern part. This spatial distribution suggests that the movement of reservoir fluid in the southern region contributes to the higher occurrence of fractures and cracks. The locations of these microseismic events are closely linked to injection and production activities and pressure changes within the wells. The calculated magnitudes of the microseismic events were relatively small in scale, as expected. These magnitude values provide insights into the size of the fractures.

Geothermal systems encompass reservoirs characterized by favorable tectonic and geological structures, as well as specific fluid compositions. Seismic waves propagating through such structures are significantly influenced by the geological framework and, in particular, the fluid content within rock fractures. Among the seismic velocities, the S-wave velocity is most sensitive to the presence of fluids and gases and exhibits the fastest response. Consequently, the VP/VS ratio, a tomographic parameter, becomes a vital quantity that can characterize subsurface fluid behavior. In this seismic tomography study, it was observed that the 3D VP and VP/VS structures of the field could be reliably resolved to a depth of 6 km. Distinct variations in the P-wave velocities were identified across different areas. Shallow depths with low VP values could be associated with young sedimentary structures, fractured formations, and porous rocks. Conversely, high VP values across all depth intervals could be attributed to volcanic and basaltic rock formations. Sections displaying low VP and low VP/VS values indicate fractured rocks with pore spaces saturated with gas or water vapor. Furthermore, sections exhibiting high VP and low VP/VS values were observed more frequently. This pattern suggests the presence of pore spaces saturated with gas or water vapor. Consequently, anomalies characterized by low VP values and high VP/VS ratios, particularly in the southern part of the field, indicate locations saturated with fluid and exhibiting high pore pressure.

REFERENCES

Asanuma H, Kumano Y, Niitsuma H, Schanz Y, Häring M (2008) Interpretation of reservoir structure from super-resolution mapping of microseismic multiplets from stimulation at Basel, Switzerland in 2006. Trans Geotherm Res Counc 32:53–58

Baria R, Baumgärtner J, Gérard A, Jung R, Garnish J (1999) European HDR research program at Soultz-sous-Forêts (France) 1987–1996. Geothermics 28:655–669

Evans KF, Genter A, Sausse J (2005) Permeability creation and damage due to massive fluid injections into granite at 3.5 km at Soultz: 1. Borehole observations J Geophys Res 110:B04203.

Fehler M. House L. Kaieda H., 1987. Determining planes along which earthquake occur: method and application to earthquakes accompanying hydraulic fracturing, J. geophys. Res., 92(B9), 9407–9414.

Geiger, L. (1910). Herdbestimmung bei Erdbeben aus den Ankunftszeiten. Nachrichten von der Königlichen Gesellschaft der Wissenschaften zu Göttingen, MathematischPhysikalische Klasse, 331-349.

Gunasekera R.C. , Foulger G.R. , Julian B.R. (2003), Reservoir Depletion At The Geysers Geothermal Area, California, Shown By Four-Dimensional Seismic Tomography,J. Geophys. Res., 108 p. 2134,

Karahan C, S. Bakrac, H. Dünya,2003. Alasehir-Kavaklıdere-Gobekli Jeotermal Enerji Arastırma Sondajının Değerlendirilmesi. Sondaj Sempozyumu MTA Ege Bolge Müdürlüğü Ve TMMOB Maden Müh. Hamdi Deliormanlı A., Seçkin C, Izmir Subesi, 10–11 Nisan 2002. Bildiriler, Pp 39–43

Karamanderesi İ. H., 1997. Salihli-Caferbeyli (Manisa İli) Jeotermal sahası potansiyeli ve geleceği.,Dünya Enerji Konseyi Türk Milli Komitesi, Türkiye 7. Enerji Kongresi teknik oturum bildiri metinleri, pp 247-261

Klein, Fred W., 2002, User's Guide to HYPOINVERSE–2000, a Fortran Program to Solve for Earthquake Locations and Magnitudes: U.S. Geological Survey Open-File Report 02-171, 123.

Koçyiğit, A., H. Yusufoğlu, E. Bozkurt, 1999. Evidence from the Gediz graben for episodic two-stage extension in Western Turkey. Journal of the Geological Society, London, 156, 605- 616.

McClure M, Horne R (2011) Investigation of injection-induced seismicity using a coupled fluid flow and rate/state friction model. Geophysics 76(6):181–198

Mukuhira Y, Dinske C, Asanuma H, Ito T, Häring MO (2016) Pore pressure behavior at the shut-in phase and causality of large induced seismicity at Basel, Switzerland. J Geophys Res Solid Earth. https://doi.org/10.1002/2016JB013338

Muksin, K. Bauer, C. Haberland,(2013),Seismic Vp And Vp/Vs Structure Of The Geothermal Area Around Tarutung (North Sumatra, Indonesia) Derived From Local Earthquake Tomography,J. Volcanol. Geotherm. Res., 260, 27-42

Tunç, S., Selek, B., Koca, B., Selek, Ü. S., Balcı, K., Yıldırım, A., & Kaypak, B. (2023). Installation of microseismic monitoring networks in geothermal fields. Journal of the Faculty of Engineering and Architecture of Gazi University, 38(3), 1307-1319.

Turhan B., Bilgiç T., Selek Ü. Balcı K., Yıldırım, A., & Kaypak, B. (2023). Jeotermal Sahalarda Mikrosismik İzleme Yöntemi ile Rezervuar Takibi, IPETGAS 2023, Oral Presentation,Ankara

Shapiro S.A.Huenges E.BormG.,1997.Estimating the crust permeability from fluid injection-induced seismic emission at the KTB site,Geophys. J. Int.,131,F15–F18.

Shapiro S.A. Rothert E. Rath V. Rindschwentner J., 2002. Characterization of fluid transport properties of reservoirs using induced microseismicity, Geophysics, 67(1), 212–220.

Yılmaz, Y., S.C. Genç, O.F. Gürer, M. Bozcu, K. Yılmaz, Z. Karacık, I. Altunkaynak, and A. Elmas, 2000. When did the western Anatolian grabens begin to develop. in Bozkurt, E., Winchester, J.A., and Piper, J.D.A., eds., Tectonics and magmatism in Turkey and the surrounding area: Geological Society of London Special Publication, 173, 353–384.

Yolal, A. and Ç. Karahan, 2010, Aydın Pamukören AP-3 Jeotermal Sondajı Kuyu Bitirme Raporu. MTA report, No. 11280.

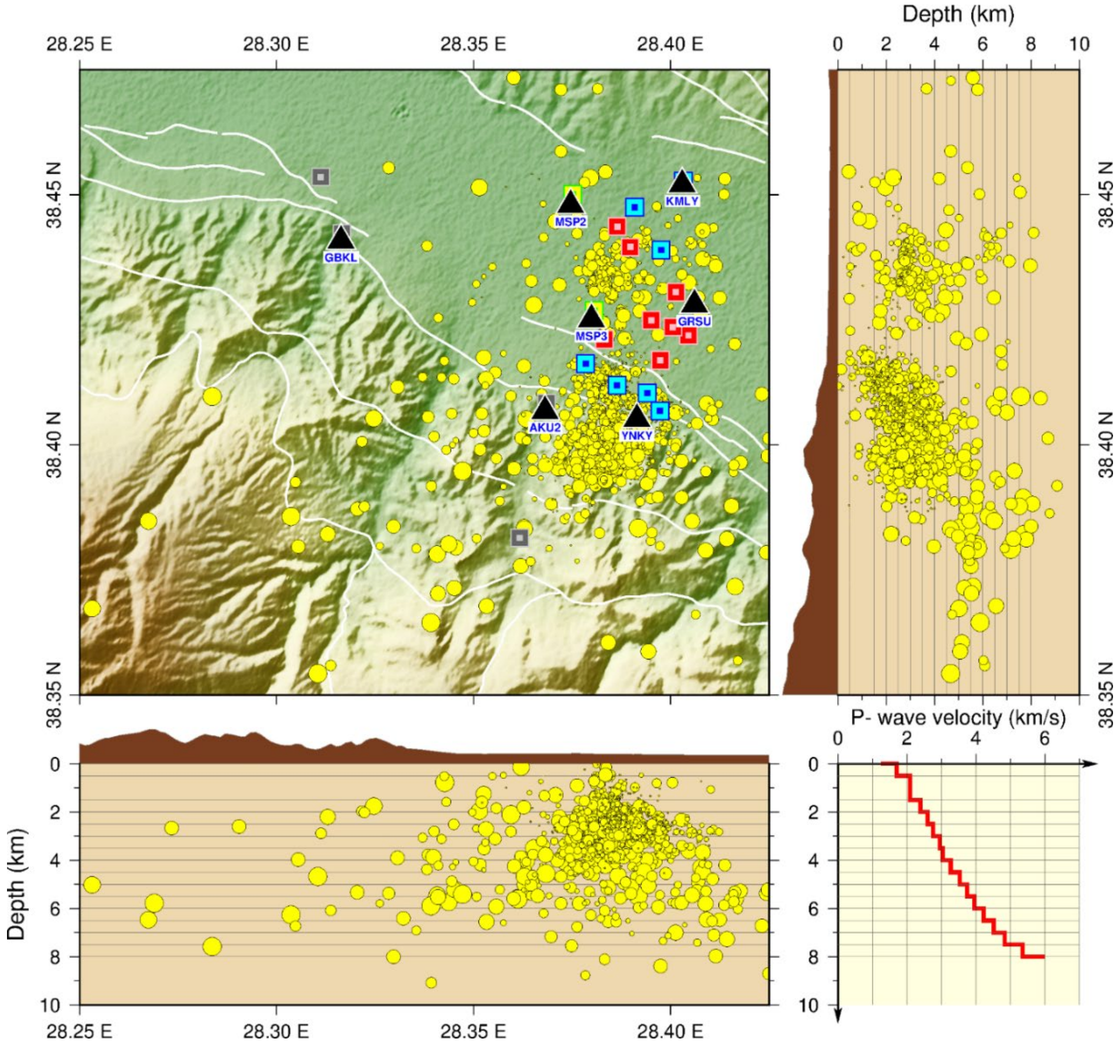

Figure6 Representation of microseismic event locations (yellow colored circles) in relation to magnitude and depth, along with the distribution of sensors (blue triangle symbols) over a two-year period. The 1-D seismic velocity model used for determining the locations is provided in the lower right corner

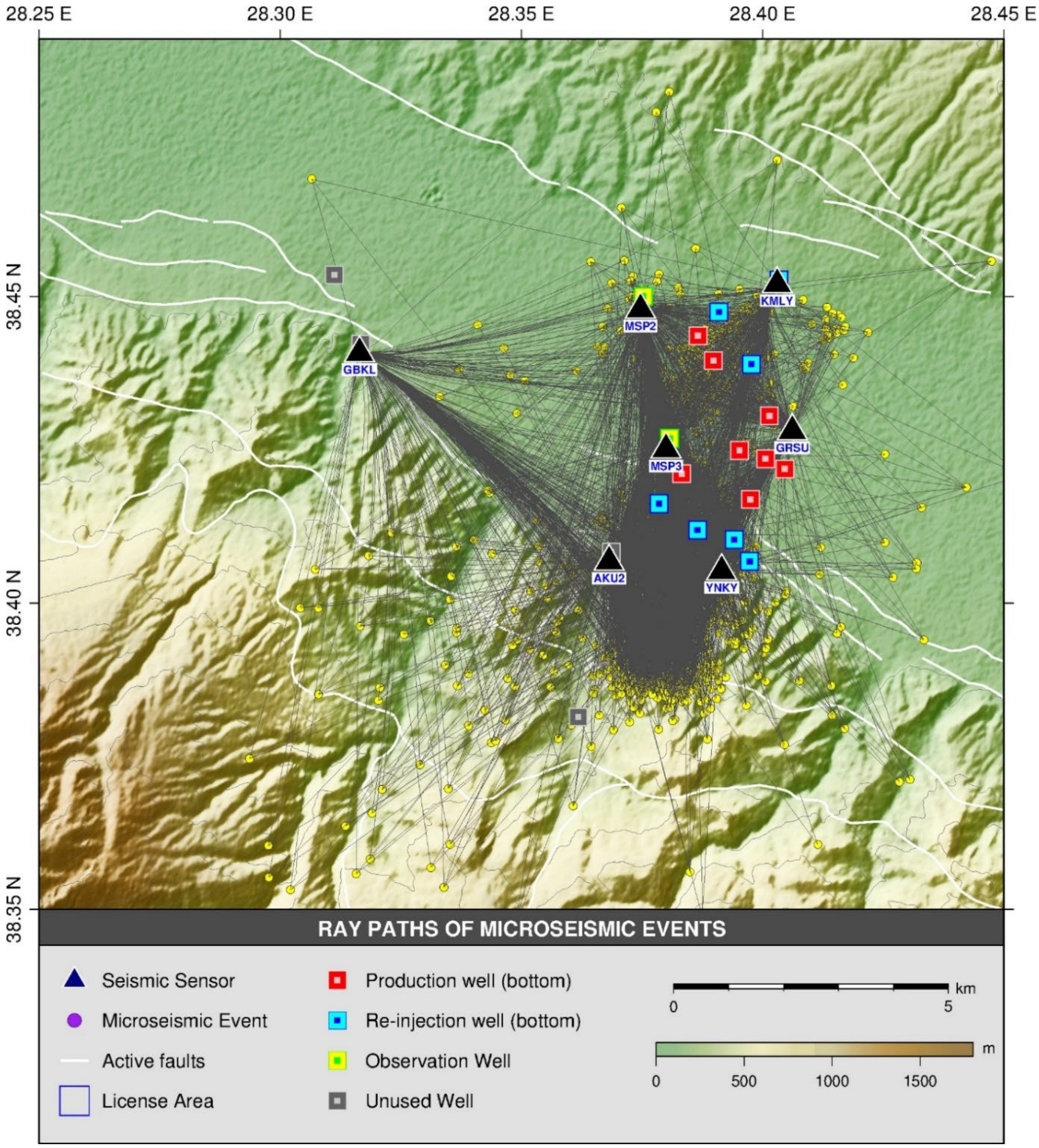

Figure7 Ray paths used in obtaining tomography results.

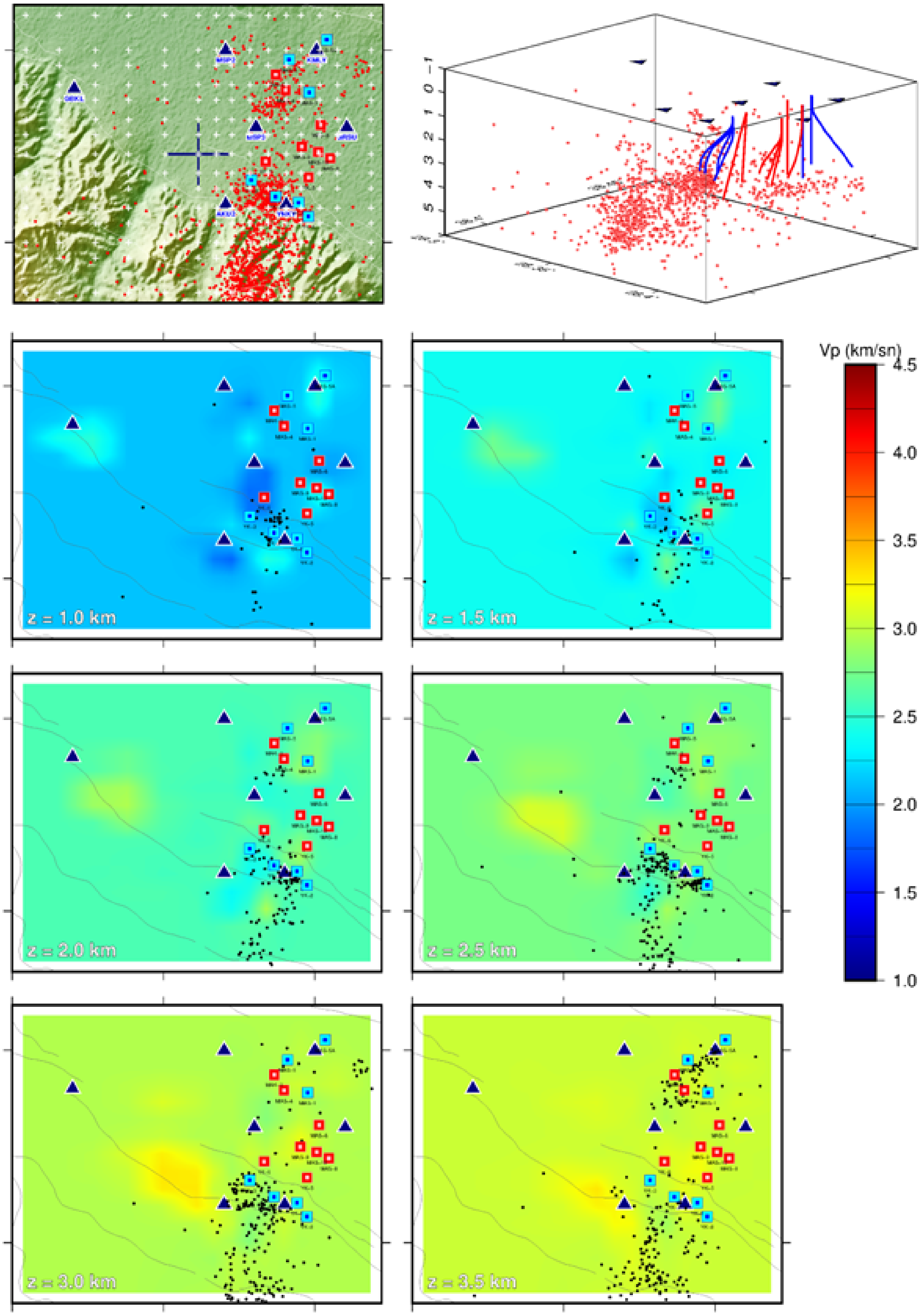

Figure8 Absolute VP layer maps obtained from the 3D inverse solution. Stations are represented by triangles in the sections, microseismic events are indicated by black/red dots, and faults are shown as white lines.

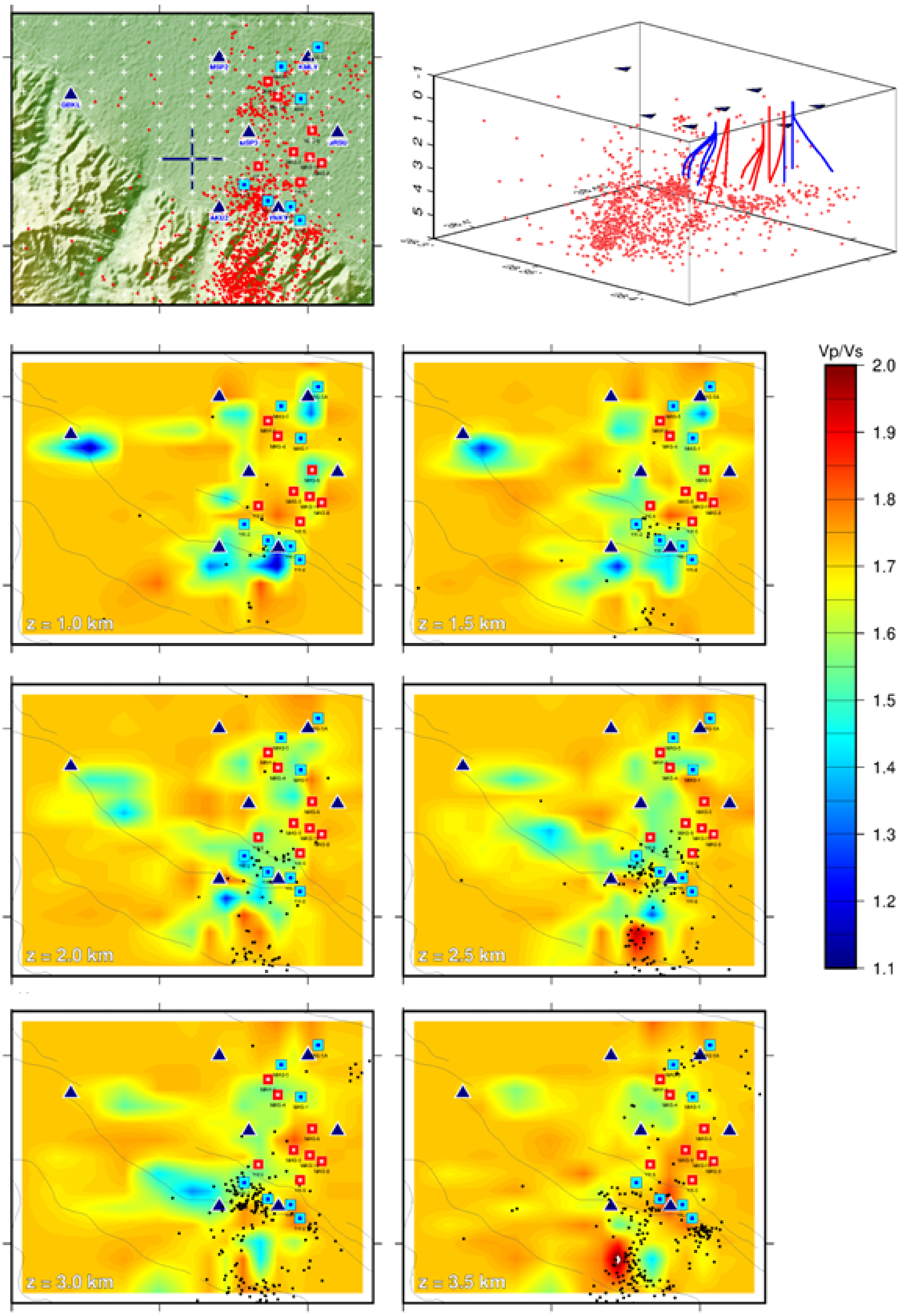

Figure9 Absolute VP/VS layer maps obtained from the 3D inverse solution. Stations are represented by triangles in the sections, microseismic events are indicated by black/red dots, and faults are shown as white lines.

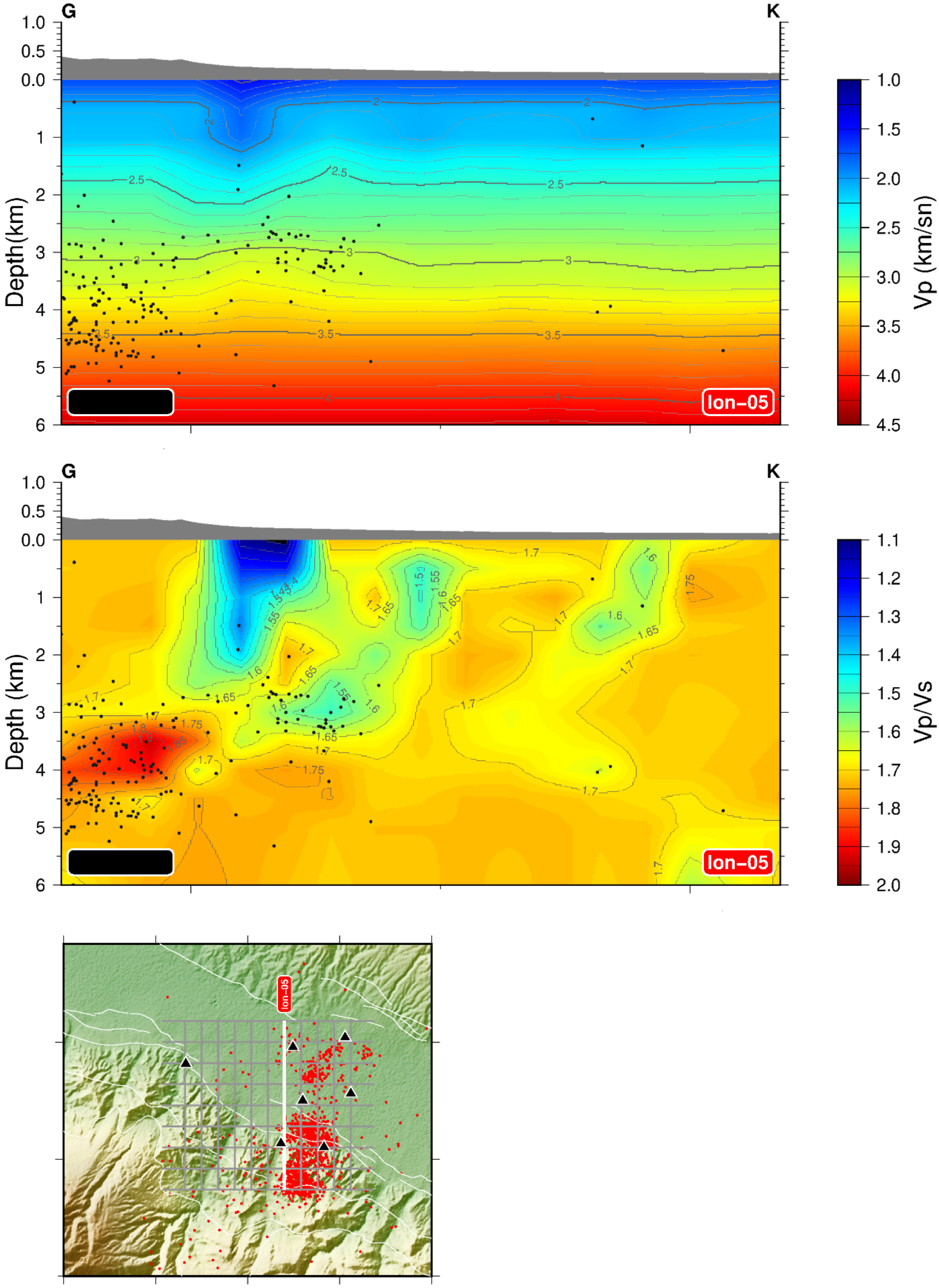

Figure10 Vertical cross-sections of absolute VP (top) and absolute VP/VS (bottom) for Profile 5. The black dots represent the locations of microseismic events projected onto the cross-section.

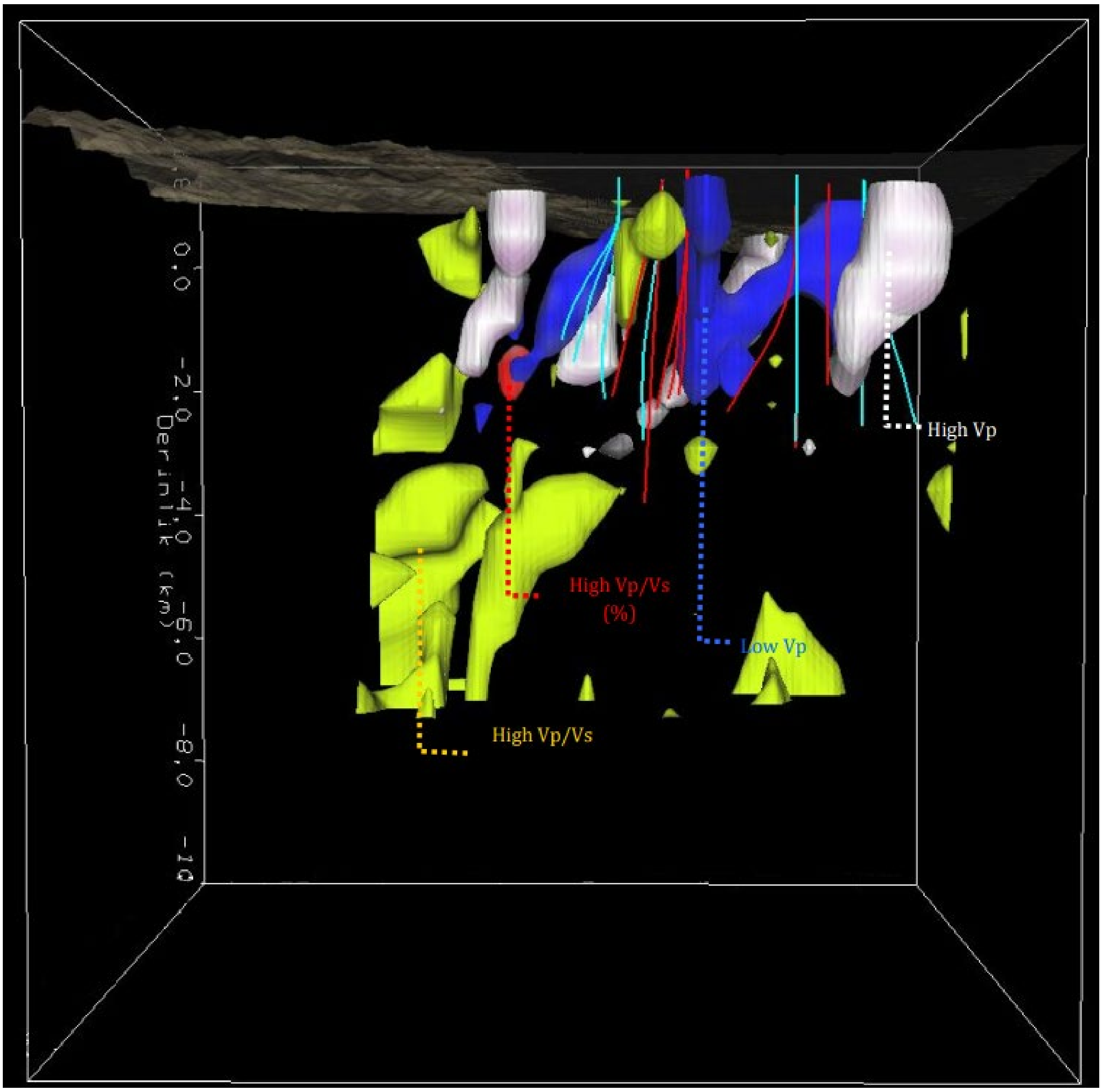

Figure11 3D Volumetric Representation of Velocity Anomalies Obtained from Tomographic Calculations (View from East to West)